Received: 30 July 2019 | Revised: 26 November 2019 | Accepted: 11 December 2019

DOI: 10.1002/asl.952

RESEARCH ARTICLE

Atmospheric Science Letters RMetS

Effective resolution in high resolution global atmospheric models for climate studies

Remko Klaver[1] | **Rein Haarsma**[1] | **Pier Luigi Vidale**[2] | **Wilco Hazeleger**[3,4]

[1]R&D Department of Weather and Climate Modeling, Royal Netherlands Meteorological Institute, De Bilt, The Netherlands

[2]Department of Meteorology, University of Reading, Reading, UK

[3]Department of Meteorology and Air Quality, University of Wageningen, Wageningen, The Netherlands

[4]Faculty of Geosciences, Universiteit Utrecht, Utrecht, The Netherlands

Correspondence
Remko Klaver, R&D Department of Weather and Climate Modeling, Royal Netherlands Meteorological Institute. PO Box 201, 3730, AE De Bilt, The Netherlands.
Email: remklaver@gmail.com

Funding information
European Commission, Horizon 2020 research programme, Grant/Award Number: 641727

Abstract

We estimate the extent of spatial scales that atmospheric models in a new generation of global climate models, used in the Coupled Model Intercomparison Project 6, are able to resolve on the basis of kinetic energy spectra, commonly referred to as the effective resolution. We examine the spectra derived from the rotational and divergent parts of the wind for six state-of-the-art global climate models that have been run with at least two horizontal resolutions. For each of the high resolution configurations, the effective resolution enhancement is less than proportional to the increase of the nominal resolution. The highest effective resolution obtained by the models in this study is roughly 200 km. This shows that the newest generation of high resolution climate models starts to resolve synoptic scales relevant for the dynamics of weather events.

KEYWORDS

atmospheric models, global climate models, horizontal resolution

1 | INTRODUCTION

Recent decades have seen a great improvement of atmospheric numerical weather prediction (NWP) and climate models. Ongoing efforts spent in model development and the increase of computational power have led to improved fidelity in the simulation of global atmospheric dynamics in numerical models (Bauer *et al.*, 2015). Due to the increase of computational power it has become possible to increase model resolution and it has been shown that several aspects of the large scale climate benefit from resolution increases (Haarsma *et al.*, 2016). Resolution increases broaden the range of scales that are resolved, which can subsequently be used for studying atmospheric dynamics. The range of the resolved scales can simply be indicated by the smallest scale that is plausibly represented in the model, which is commonly referred to as the effective resolution. The effective resolution is usually determined by analysis of the kinetic energy (KE) spectrum (Skamarock, 2004). In this study we take the same approach to determine the effective resolution for a set of state-of-the-art global climate models.

It is known from observations that the spectral magnitude decreases with scale. In the upper troposphere, the slope roughly follows a power law of k^{-3} in the synoptic range of scales and then transitions to a shallower

$k^{-5/3}$-law in the mesoscale (Lindborg, 1999). Callies *et al.* (2014) derived from measurements between 30°N and 60°N that the k^{-3}-law of the spectrum at the large scale can be attributed to the rotational wind, which dominates the KE spectrum at the large scales. The rotational and divergent components of the spectrum converge at the mesoscale, with both components following the mesoscale $k^{-5/3}$-law. Note that these latitudes are a major influence on the global KE spectrum due to the generation of KE at the midlatitudes from baroclinic instability.

The shape and transition of the KE spectrum is a result of generation of KE predominantly in the synoptic range (wavelengths 1,000–4,000 km) and the scale dependent dynamical constraints in the atmospheric cascade of KE. The k^{-3}-law in the synoptic range is commonly attributed to a downscale enstrophy cascade constrained by the Earth's rotation and the stratification of the atmosphere, known as geostrophic turbulence (Charney, 1971). The $k^{-5/3}$-law in the mesoscale arises from a downscale energy cascade in a regime that is dominated by inertia-gravity waves (Callies *et al.*, 2014).

It is well known (Pielke, 1991; Laprise, 1992) that models do not realistically simulate the Earth's atmosphere at scales that are close to their mesh size. Parameterizations, numerical diffusion, interpolation, aliasing, and anti-aliasing filters lead to dissipation of KE and consequently to a breakdown of the atmospheric power laws. This study addresses the energy spectra of atmospheric models used in contemporary climate and earth system model intercomparisons, in particular Coupled Model Intercomparison Projects 5 (Taylor *et al.*, 2011) and 6 (Eyring *et al.*, 2016). The horizontal grid resolution spans from 250 to 25 km. The finest resolutions start to resolve synoptic scales. Because these model simulations are the basis of many diagnostic studies, it is relevant to know the effective resolutions of these models. The effective resolution can be interpreted as a *dynamical* resolution. In contrast, the nominal resolution, refers merely to the mesh size of the model's grid. Scales smaller than the effective resolution are incorrectly simulated and should be disregarded in the context of interpretational climate studies such as climate change, climate variability, weather extremes, and weather regimes.

Previous studies have focused on various resolution configurations of a single model using spectra that were derived from Fourier transforms. For instance, Skamarock (2004) determined the effective resolution of a limited area NWP model using vertically integrated spectra, while Abdalla *et al.* (2013) determined the effective resolution of a global NWP model using data from a limited area. We present a diagnostic for the effective resolution that uses global data and is applicable irrespective of the models' grids. Section 2 describes the methodology

TABLE 1 Models and each of their grid configurations (13 in total) examined in this study

Model-Version	Type	Grid	$\bar{L}_{box}$ (km)	l_{eff}	L_{eff} (km)	$L_{eff}/\bar{L}_{box}$
HadGEM3-GC31-LM	Grid point	145 × 192	217	≤32	≥625	≥2.9
HadGEM3-GC31-MM	Grid point	325 × 432	96.7	55	364	3.8
HadGEM3-GC31-HM	Grid point	769 x 1,024	40.8	108	185	4.5
CMCC-CM2-HR4	Grid point	192 × 288	153	35	571	3.7
CMCC-CM2-VHR4	Grid point	768 × 1,152	38.2	110	182	4.8
ECMWF-IFS-LR	Spectral	Reduced TCO199	79.6	79	253	3.2
ECMWF-IFS-HR	Spectral	Reduced TCO399	40.4	108	185	4.6
EC-Earth3	Spectral	Reduced TL255	107	57	351	3.3
EC-Earth3-HR	Spectral	Reduced TL511	54.2	84	238	4.4
MPIESM-1-2-HR	Spectral	TQ127	134	55	364	2.7
MPIESM-1-2-XR	Spectral	TQ255	66.9	78	256	3.8
CNRM-CM6-0	Spectral	Reduced TL127	207	≤32	≥625	≥3.0
CNRM-CM6-0-HR	Spectral	Reduced TL359	75.3	64	313	4.2

Notes: For the grid point models, the third column denotes the number of grid points (latitudes × longitudes). For the spectral models, it specifies both the spectral representation of variables and the Gaussian grids. The first letter (T) refers solely to the spectral representation and is disregarded in this study. The second letter refers to the grids' ability to transform either linear (L), quadratic (Q), or cubic (C) terms without aliasing, which requires 2, 3, or 4 grid points for the smallest wavelength, respectively. The number refers to the truncation (largest) wavenumber. The term "reduced" refers to a reduction toward the poles of the number of zonal grid points. Furthermore, ECMWF-IFS uses a octahedral (O) grid, which refers to the pattern of the grid points. The representative grid box distance $\bar{L}_{box}$ is an area weighted mean grid box diagonal, which indicates the nominal resolution of the models. We refer to the supporting information (Appendix S1, Figure S1) for its calculation and more details on the different grids. The effective resolution is denoted in the three rightmost columns, in terms of wavenumber l_{eff}, the corresponding spatial scale L_{eff} and the ratio of the latter with the representative grid box distance.

and data for this study. Section 3 describes the results. Section 4 is the discussion.

2 | DATA AND METHODOLOGY

2.1 | Models and data

We determine the effective resolution for a set of high resolution climate models (Table 1) in atmosphere-only configuration. This set consists of the first simulations to follow the CMIP6 HighResMIP protocol. We study six global models, each of which is run at two or three horizontal resolutions. The nominal resolution ranges between 25 and 250 km according to the CMIP6 standard. The nominal resolution of the models is indicated by the representative grid box distance $\bar{L}_{\mathrm{box}}$ (Table 1), that is, an area weighted mean grid box diagonal. We refer to the supporting information (Appendix S1, Figure S1) for the calculation and more details on the different grids. A more detailed description of models and experiment is given in Roberts (2019) and references therein. We analyze the mean spectra from six hourly values of the horizontal wind at 250 and 500 hPa during 4 months (March, June, September, and December 2014).

2.2 | Spectra

We compute the global spectrum from the spherical harmonic (SH) coefficients of the divergence ($d_{l,\,m}$) and vorticity ($\zeta_{l,\,m}$) of the horizontal wind (Lambert, 1984)

$$E^{l,m} = \frac{a^2}{2l(l+1)}\left(\left|\zeta_{l,m}\right|^2 + \left|d_{l,m}\right|^2\right) \tag{1}$$

Here, a is the radius of the Earth. We determine the spectrum as a function of total wavenumber l, that is, the sum of Equation (1) over zonal wavenumber m

$$E^l = \sum_{m=-l}^{l} E^{l,m} \tag{2}$$

The spatial scale and total wavenumber l are related through the Laplacian $\nabla^2 Y^{l,m} = \frac{-l(l+1)}{a^2} Y^{l,m}$. We define the half wavelength, or eddy scale ΔS, as (Burgess *et al*., 2012)

$$\Delta S = \pi\sqrt{\frac{a^2}{l(l+1)}} \approx \frac{\pi a}{l} \approx \frac{20.000}{l} \tag{3}$$

in km. For the spectral models EC-Earth3 and MPI-ESM-1-2, we use a software package (Schaeffer, 2013) for the computation of the spectral coefficients in Equation (1). In Appendix S2 we describe the computation of the spectral coefficients for the other models, specifically the grid point models CMCC-CM2 and HadGEM-GC31 and the spectral models ECMWF-IFS and CNRM-CM6-0. Appendix S2 includes a verification of accuracy of the derived spectra (Figure S2).

2.3 | Method

We determine the effective resolution as the scale, beyond which, the KE spectrum indicates an apparent influence of the finite resolution. This is diagnosed from steepening of the spectral slope. The steepening of the spectral slope occurs gradually, therefore, the transition between the resolved and unresolved scales is a gradual one. An essential characteristic of this transition between the resolved and unresolved scales is a progressive deterioration of the spectrum with increasing wavenumber. Therefore, it is essential that, beyond the effective resolution, the spectrum steepens progressively with increasing wavenumber, toward a spectral slope that deviates strongly from the observed power laws.

The spectral slope is determined by a fit over a range of 20 wavenumbers (Appendix S3). Steepening of the slope, indicated by the increase of the exponent n of the fitted function $y = Cl^{-n}$, is indicative of steepening at the largest wavenumber in the range, when the slope is more or less constant throughout the rest of the wavenumbers in that particular range. This method is feasible to indicate steepening at wavenumbers $l \geq 32$ ($\Delta S = 625$ km), since the spectrum is shallower than the approximate k^{-3} power law at the smallest wavenumbers $l < 13$.

We use global KE spectra with spherical harmonics as basis functions. For each model and resolution configuration, we indicate suspicious steepening of the KE spectra separately for the *rotational* and the *divergent* parts of the wind. The use of global spectra, rather than spectra representative for a limited area, ensures a consistent comparison between the spectra, even though the latitudinal dependence of the grid point distance differs between the models (Appendix S1).

Steepening of either the rotational or the divergent spectrum near the tropopause is not in accordance with observations (Callies *et al*., 2014). Furthermore, the influence of resolution should also be apparent at lower levels in the atmosphere. We determine the effective resolution as the wavenumber at which steepening is diagnosed for

at least two out of three spectra (one at 500 hPa and two at 250 hPa), specifically the divergent spectrum at 250 hPa and the rotational spectra at 250 and 500 hPa. Steepening of a second spectrum (out of three) enhances the confidence in the model's apparent inability to accurately simulate the KE content of the wind beyond that wavenumber. The spectra of the divergent part of the wind at 500 hPa are disregarded, because these spectra appear to steepen at all scales (Figure S3).

For the detection of steepening of the spectra, we pick a minimum degree of steepening, specifically an increase of the fitted exponent by 25% for an increase of wavenumber by a factor 2. This is an ad hoc and somewhat arbitrary value, which has been chosen as it appears to work well for detecting the effective resolution of the studied models. The numerical value (25%) prevents detection of steepening that is only marginal. The use of a second spectrum to confirm the steepening reduces the sensitivity to the precise value of 25%. Most importantly, the goal is to indicate the suspicious character of the spectra at wavenumbers beyond the effective resolution. This degree of steepening is compelling evidence of the influence of resolution.

We emphasize, that it is not in our scope, to study the fidelity of the spectra in the resolved range of scales. Notably, the presented diagnostic of the effective resolution on the basis of steepening is not directly affected by the spectral slope in the resolved range of scales.

3 | RESULTS

Figure 1a–c,g–i depict the 250 hPa divergent (dark blue) and both the 250 and 500 hPa rotational (red and green, respectively) KE spectra. The derived spectral slopes are depicted in panels d–f, j–l in corresponding colors. Solid lines correspond to the high resolution configuration, while the dashed lines to a lower resolution (Table 1). HadGEM-GC31 is run at three horizontal resolution configurations, of which, the lowest resolution is depicted by the dotted lines. The x-axis indicates the wavenumber (bottom) and the corresponding half wavelength (top), that is, eddy scale, and is the same for all panels.

We plot the KE spectra as l^{-3}-compensated spectra, that is, a multiplication of the spectra with wavenumber l to the power third. A horizontal spectrum therefore indicates a spectrum that follows a power law of k^{-3} (solid orange line), which is the reference slope for the KE spectrum of the rotational part of the wind at the large (synoptic) scales. This presentation helps to better visualize differences between the spectra in terms of both the spectral amplitude and the slope, because the amplitude decreases by several orders of magnitude in the examined range of wavenumbers (Figure S3 depicts the same figure without this compensation). Note that a power law on logarithmic axes yields a straight line, therefore, curvature of the compensated spectra is solely due to curvature of the original spectrum. The panels also depict power laws $k^{-5/3}$ (solid light blue line) and k^{-3} (solid orange line) and an additional reference slope of a power law with an exponent that is 10% larger than these slopes (dash-dotted lines in corresponding colors).

The spectra are not depicted up to the truncation wavenumber, in order to reduce computational effort. Moreover, the computation of the spectral coefficients on a regular grid is not accurate at very large wavenumbers. Note that the spectral slopes do not substantially differ between the different months and therefore the effective resolution is a robust (time invariant) feature of the models (not shown).

The effective resolution is determined from the spectral slope depicted in panels d-f, j–l, which use the same color coding and line style as the spectra. The vertical lines indicate the wavenumber beyond which we find steepening of the spectral slope. In addition, the panels include straight skewed lines for each vertical line, which indicate the increase of the exponent by 25% for an increase of the wavenumber by a factor 2. These lines intercept the corresponding spectrum at the vertical line and show that the spectra are steepening to a lesser degree at smaller wavenumbers and to a larger degree at larger wavenumbers. Those wavenumbers (vertical lines), are also indicated in the panels that depict the corresponding spectra. Note that the color and line style of both the vertical lines and the skewed lines are the same as the corresponding spectrum.

In the panels that depict the spectra (a–c, g–i) a vertical black line (corresponding line style) indicates the effective resolution. Specifically, this is the wavenumber, at which, two of the three spectra are detected to steepen.

For most of the studied models, the spectrum of the rotational wind at 500 hPa is one of the two spectra that are detected to steepen. Therefore, the influence of resolution is evident both at 250 hPa as well as at 500 hPa. For the two models, in which the spectrum of the rotational wind at 500 hPa steepens at a larger wavenumber than both spectra at 250 hPa, that is, CMCC-CM2-HR4 and CNRM-CM6-0-HR, the 500 hPa spectra appear to confirm the influence of resolution. For the former, CMCC-CM2-HR4, the influence of resolution at 500 hPa is confirmed by a marked deviation with the higher resolution configuration. Specifically, by an absence of shallowing, that is, a decrease of the exponent with increasing wavenumber, in the lower resolution configuration, in contrast with the higher resolution configuration. This is visible by the difference beyond the effective

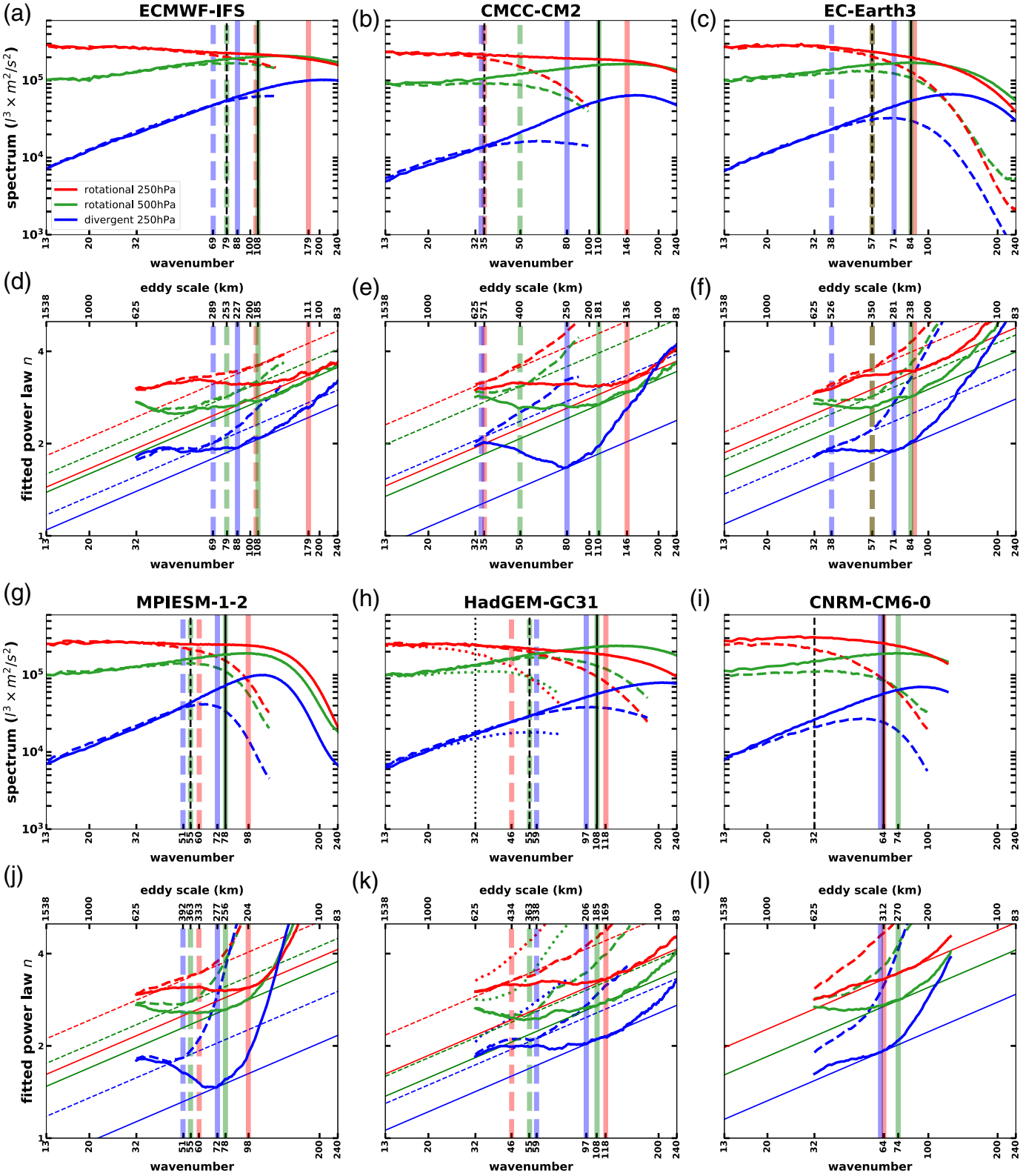

FIGURE 1 l^{-3}-compensated monthly mean global kinetic energy (KE) spectra derived from the rotational (red) and divergent (blue) parts of the wind at 250 hPa and from the rotational part of the wind at 500 hPa (green) for each of the resolution configurations of ECMWF-IFS (a), CMCC-CM2 (b), HadGEM-GC31 (c), MPIESM-1-2 (g), EC-Earth3 (h), and CNRM-CM6-0 (i). Dashed lines correspond to the low resolution and solid lines correspond to the high resolution configurations. HadGEM-GC31 includes a third (lower) resolution depicted as dotted lines. Black vertical lines depict the effective resolution. Panels d–f,j–l depict the exponent of the spectral slope as a function of wavenumber. The diagnosed steepening for each of the spectra is depicted by semi-transparent vertical lines. At these wavenumbers, the straight skewed lines intersect the curves that depict the exponent of the spectral slope. Color and line style correspond to the spectra. The vertical and skewed colored lines are not included for HadGEM-GC31-LM and CNRM-CM6-0 (low resolution)

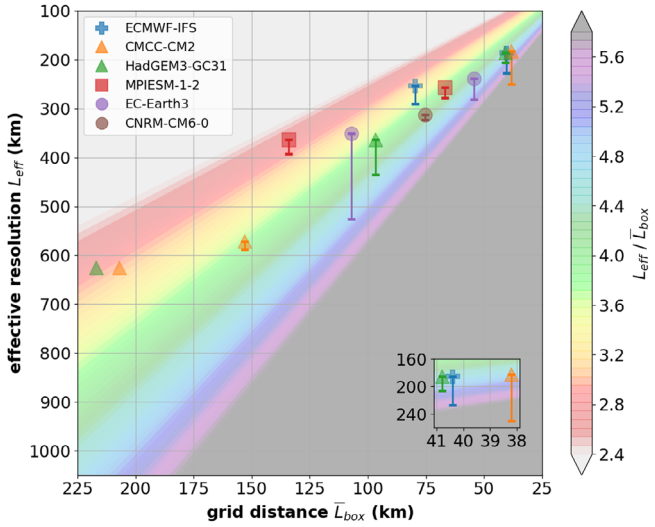

FIGURE 2 Scatter plot of the effective resolution L_{eff} versus the representative grid box distance $\bar{L}_{\text{box}}$. Color shading depicts the scaling between effective resolution and representative grid box distance (i.e., y/x). The markers depict the effective resolution, that is, where steepening is diagnosed for two out of the three spectra. The error bar denotes the range of scale at which steepening is diagnosed for one of the three spectra. For the low resolution configurations HadGEM-GC31-LM and CNRM-CM6-0, the markers depict an upper limit of the effective resolution. Error bars are not depicted for these two models. The inlay in the lower right corner provides a zoom of the models ECMWF-IFS-HR, CMCC-CM2-VHR4, and HadGEM-GC31-HM

resolution ($l_{\text{eff}} = 35$) between the dashed (CMCC-CM2-HR4) and solid (CMCC-CM2-VHR4) lines in green (panels b, e). For the latter, CNRM-CM6-0-HR, the green solid line is steepening substantially, even though this steepening is slightly less severe than the detection criterium (depicted by the skewed straight lines). For each of the studied models, therefore, the effective resolution (black vertical lines) indicates the scale, beyond which, both the 250 and 500 hPa KE content appear affected by the finite resolution.

For the models HadGEM-GC31-LM (panels h, k) and CNRM-CM6-0-LR (panels i, l), each of the three studied spectra appear to deviate substantially from their higher resolution configurations at wavenumber $l = 32$. Since this is the smallest wavenumber that is feasible for our method of detecting steepening (Appendix S3), this wavenumber is an upper limit with regard to the effective resolution. Therefore, these two models have an effective resolution $l_{\text{eff}} \leq 32$ (eddy scale $\Delta S \geq 625$ km). Vertical lines that depict steepening are not included for these two model configurations.

In a few cases, such as the 250 hPa rotational spectra of MPI-ESM-1-2-HR (which refers to the low resolution configuration) and HadGEM-GC31-MM, the detected steepening is rather sensitive to the degree of steepening that we choose to diagnose the effective resolution. In both cases, however, this sensitivity does not substantially influence the value at which the steepening is confirmed by a second spectrum (which is equivalent of the median of the three wavenumbers at which steepening is detected). Consequently, the sensitivity of the diagnosed effective resolution to the value of 25% is only marginal.

At 250 hPa, the spectrum derived from the divergent part of the wind shows a sudden and pronounced steepening for most models and in most cases it is detected at a smaller wavenumber than the steepening of the spectrum derived from the rotational wind. The steepening of the rotational part of the spectrum of the studied models is comparatively less sudden and is less pronounced. This difference in the appearance of steepening, suggests that the dissipative influence of resolution on the spectrum at the smallest resolved scales differs between the rotational and divergent parts of the wind. This may be related to the different nature of the KE cascade of the rotational and the divergent KE (Augier and Lindborg, 2013).

Figure 2 depicts a scatter plot of the effective resolution and the representative grid box distance for each of the models. The markers are equal for the different resolution configurations of each model. The error bars indicate the range of wavenumbers, at which, only one spectrum steepens (out of the three).

Table 1 includes the effective resolution as a ratio over the grid distance ($L_{\text{eff}}/L_{\text{box}}$). This ratio allows for a comparison to previous studies of the effective resolution, for example, Skamarock (2004) ($L_{\text{eff}} \approx 7\Delta x$) or Abdalla *et al.* (2013) ($L_{\text{eff}} \approx 8\Delta x$). Here, the grid distance $\Delta x \approx \bar{L}_{\text{box}}/\sqrt{2}$ and the numerical values express length scale in units of full wavelengths instead of eddy scale (half wavelength). In addition, the fact that this ratio varies within 2.7–4.8 can be used as a crude a priori estimate of the effective resolution for climate models within the presented range of resolutions, since this set of models encompasses a rather various set of model grids (Appendix S1). Interestingly, this ratio ($L_{\text{eff}}/L_{\text{box}}$) is consistently larger for the high resolution configurations than for the low resolution counterparts within each of the models. It is not in the scope of the present diagnostic study to explain this result (Section 4).

4 | DISCUSSION

We have determined the effective resolution for a set of current state-of-the-art climate models. The highest effective resolution is roughly 200 km ($l = 108$–110) and is obtained by HadGEM-GC31-HM, CMCC-CM2-VHR4, and ECMWF-IFS-HR. This indicates that the resolution

enhancement achieved in these models enables resolving the synoptic scales that are relevant for the dynamics of weather events. The length scale of the effective resolution of the analyzed models is between 2.7 and 4.8 times an area weighted mean grid box diagonal.

The methodology differs from previous studies that analyze the KE spectra of a single NWP model (Skamarock, 2004; Abdalla *et al*., 2013) in order to consistently estimate the effective resolution for the different models. First, the effective resolution is determined from global KE spectra, because the grids employed in the examined models are associated with different latitudinal dependence of the grid distance. Second, the presented diagnostic is based on the deviation from the slope in the resolved range. This is useful, because of substantial differences between the models in the resolved range. Moreover, the correspondence with observed spectra is not direct. Hence, the uncertainty of analogous atmospheric spectra is considerable.

Third, we separately analyze the KE spectra associated with the rotational and divergent parts of the wind, while previous studies used the total KE spectrum to diagnose the effective resolution. For most of the models at 250 hPa, the divergent part of the spectrum steepens at a smaller wavenumber than the rotational spectrum and, in addition, in a comparatively pronounced manner. The steepening of the divergent spectrum is not as evident in the total spectrum, since, at the wavenumbers relevant for the range of resolutions of the climate models in this study, the spectral amplitude of the rotational wind is substantially larger than the amplitude associated with the divergent wind. We emphasize that the spectra of both the rotational and the divergent wind require realistic power laws for simulating the atmosphere with fidelity. This difference between the steepening of the rotational and divergent parts of the spectrum indicates a benefit of analyzing the rotational and divergent parts of the spectrum separately, and suggests that the divergent spectrum is particularly useful for diagnosis of the effective resolution.

We find that the ratio of the effective resolution over the grid distance is consistently larger for the high resolution configurations than for the low resolution counterparts within each of the models. An explanation of this result is outside the scope of this study, but points toward a scale dependency of how nominal resolution is related to effective resolution. Sensitivity studies or the application of the presented diagnostic to a wider range of model resolutions may elucidate the relation between effective resolution and grid distance. This study, however, does not aim to provide an understanding of the impact of resolution nor does is attempt to justify the fidelity of the scales larger than the effective resolution. Rather, the presented methodology to derive the effective resolution aims to provide a diagnostic that is applicable for a variety of climate models. The authors caution that the use of an integrated quantity such as the global averaged kinetic energy, might obscure the possibility that the effective resolution is different for different meteorological phenomena, such as midlatitude storms versus equatorial updrafts.

ACKNOWLEDGEMENTS

We thank Chris Roberts (ECMWF) for providing additional data to verify the accuracy of the spectra. PRIMAVERA project members (R.K., R.H. and P.L.V.) acknowledge funding received from the European Commission under grant agreement 641727 of the Horizon 2020 research programme.

ORCID

Remko Klaver https://orcid.org/0000-0003-3722-6161

REFERENCES

Abdalla, S., Isaksen, L., Janssen, P. and Wedi, N. (2013) Effective spectral resolution of ecmwf atmospheric forecast models. *ECMWF Newsletter*, 137, 19–22 Available at: https://www.ecmwf.int/node/17358.

Augier, P. and Lindborg, E. (2013) A new formulation of the spectral energy budget of the atmosphere, with application to two high-resolution general circulation models. *Journal of the Atmospheric Sciences*, 70, 2293–2308. https://doi.org/10.1175/JAS-D-12-0281.1.

Bauer, P., Thorpe, A. and Brunet, G. (2015) The quiet revolution of numerical weather prediction. *Nature*, 525, 47 EP–55. https://doi.org/10.1038/nature14956.

Burgess, B.H., Erler, A.R. and Shepherd, T.G. (2012) The troposphere-to-stratosphere transition in kinetic energy spectra and nonlinear spectral fluxes as seen in ecmwf analyses. *Journal of the Atmospheric Sciences*, 70, 669–687. https://doi.org/10.1175/JAS-D-12-0129.1.

Callies, J., Ferrari, R. and Bühler, O. (2014) Transition from geostrophic turbulence to inertia–gravity waves in the atmospheric energy spectrum. *Proceedings of the National Academy of Sciences of the United States of America*, 111, 17033–17038. https://doi.org/10.1073/pnas.1410772111.

Charney, J.G. (1971) Geostrophic turbulence. *Journal of the Atmospheric Sciences*, 28, 1087–1095. https://doi.org/10.1175/1520-0469.

Eyring, V., Bony, S., Meehl, G.A., Senior, C.A., Stevens, B., Stouffer, R.J. and Taylor, K.E. (2016) Overview of the coupled model intercomparison project phase 6 (cmip6) experimental design and organization. *Geoscientific Model Development*, 9, 1937–1958. https://doi.org/10.5194/gmd-9-1937-2016.

Haarsma, R.J., Roberts, M.J., Vidale, P.L., Senior, C.A., Bellucci, A., Bao, Q., Chang, P., Corti, S., Fučkar, N.S., Guemas, V., von Hardenberg, J., Hazeleger, W., Kodama, C., Koenigk, T., Leung, L.R., Lu, J., Luo, J.-J., Mao, J., Mizielinski, M.S., Mizuta, R., Nobre, P., Satoh, M., Scoccimarro, E., Semmler, T., Small, J. and von Storch, J.-S. (2016) High resolution model

intercomparison project (highresmip v1.0) for cmip6. *Geoscientific Model Development*, 9, 4185–4208. https://doi.org/10.5194/gmd-9-4185-2016.

Lambert, S.J. (1984) A global available potential energy-kinetic energy budget in terms of the two-dimensional wavenumber for the fgge year. *Atmosphere-Ocean*, 22, 265–282. https://doi.org/10.1080/07055900.1984.9649199.

Laprise, R. (1992) The resolution of global spectral models. *Bulletin of the American Meteorological Society*, 73, 1453–1455. https://doi.org/10.1175/1520-0477-73.9.1453.

Lindborg, E. (1999) Can the atmospheric kinetic energy spectrum be explained by two-dimensional turbulence? *Journal of Fluid Mechanics*, 388, 259–288. https://doi.org/10.1017/S0022112099004851.

Pielke, R.A. (1991) A recommended specific definition of "resolution". *Bulletin of the American Meteorological Society*, 72, 1914–1914. https://doi.org/10.1175/1520-0477-72.12.1914.

Roberts, M.J. (2019) Impact of model resolution on tropical cyclone simulation using the highresmip - primavera multi-model ensemble. *Journal of Climate*. https://doi.org/10.1175/JCLI-D-19-0639.1.

Schaeffer, N. (2013) Efficient spherical harmonic transforms aimed at pseudospectral numerical simulations. *Geochemistry, Geophysics, Geosystems*, 14, 751–758. https://doi.org/10.1002/ggge.20071.

Skamarock, W.C. (2004) Evaluating mesoscale nwp models using kinetic energy spectra. *Monthly Weather Review*, 132, 3019–3032. https://doi.org/10.1175/MWR2830.1.

Taylor, K.E., Stouffer, R.J. and Meehl, G.A. (2011) An overview of cmip5 and the experiment design. *Bulletin of the American Meteorological Society*, 93, 485–498.

SUPPORTING INFORMATION

Additional supporting information may be found online in the Supporting Information section at the end of this article.

How to cite this article: Klaver R, Haarsma R, Vidale PL, Hazeleger W. Effective resolution in high resolution global atmospheric models for climate studies. *Atmos Sci Lett*. 2020;1–8. https://doi.org/10.1002/asl.952